



Article

Wafer-Scale Fabrication and Assembly Method of Multichannel Microelectrode Arrays for ECoG Application

Cong Wang ^{1,*}, Yu-Chen Wei ¹, Ho-Kun Sung ², Alok Kumar ¹, Zhong-Liang Zhou ¹, Dan-Qing Zou ¹, Cheng-Peng Jiang ³, Guo-Feng Yan ³, Jee-Hyun Choi ⁴ and Rajendra Dhakal ⁵

¹ School of Electronics and Information Engineering, Harbin Institute of Technology, Harbin 150001, China; weiyuchen@hit.edu.cn (Y.-C.W.); kalok2705@gmail.com (A.K.); zhouzhongliang@hit.edu.cn (Z.-L.Z.); zoudanqing@hit.edu.cn (D.-Q.Z.)

² Korea Advanced Nano Fab Center (KANC), Suwon 16229, Korea; hokun.sung@kanc.re.kr

³ Research Center for Smart Sensing, Zhejiang Lab, Hangzhou 310000, China; cpjiang@zhejianglab.com (C.-P.J.); yangf@zhejianglab.com (G.-F.Y.)

⁴ Center for Neural Science, Korea Institute of Science and Technology (KIST), Seoul 25451, Korea; jeehyunchoi.kist@gmail.com

⁵ Department of Computer Science and Engineering, Sejong University, Seoul 05006, Korea; rajendra@sejong.ac.kr

* Correspondence: kevinwang@hit.edu.cn

Abstract: High density electrocorticography (ECoG)-based microelectrode arrays (MEAs) are fabricated to timely record the neural activities to provide the fundamental understanding in neuroscience and biomedical engineering. This paper aims to introduce a device-based concept and wafer-scale fabrication process for MEAs. Flexible and biocompatible polyimide is applied on MEAs to bear all possible stress and strain. Detailed fabrication key techniques, including surface treatment, polyimide stability measurement, evaporation process, and curing conditions, have been discussed thoroughly. Moreover, the fabricated polyimide-based MEAs are surface-mounted on well-packaged printed circuit boards (PCBs) via a slot-type connector without any additional wire bonding to make the signal recording process easier. An absence seizure was recorded during the in vivo test, which shows the availability of signal recording based on the presented MEAs. The proposed MEAs could be remained at the skull, while the connector and PCBs can be disassembled apart. Therefore, the testing sample will get less suffering. To verify the robustness of the fabricated MEAs, the impedance properties were characterized using electrochemical impedance spectroscopy. The measured results indicate an average impedance of 12.3 ± 0.675 k Ω at 1 kHz. In total, 10 groups of MEAs were sample tested, and over 90% of the total 60 channels per 1-MEAs operated efficiently.

Keywords: microelectrode arrays; wafer-scale fabrication; multichannel; neuronal recordings



Citation: Wang, C.; Wei, Y.-C.; Sung, H.-K.; Kumar, A.; Zhou, Z.-L.; Zou, D.-Q.; Jiang, C.-P.; Yan, G.-F.; Choi, J.-H.; Dhakal, R. Wafer-Scale Fabrication and Assembly Method of Multichannel Microelectrode Arrays for ECoG Application. *Electronics* **2021**, *10*, 316. <https://doi.org/10.3390/electronics10030316>

Academic Editor: Andrzej Czyżewski

Received: 14 January 2021

Accepted: 26 January 2021

Published: 29 January 2021

Publisher's Note: MDPI stays neutral with regard to jurisdictional claims in published maps and institutional affiliations.



Copyright: © 2021 by the authors. Licensee MDPI, Basel, Switzerland. This article is an open access article distributed under the terms and conditions of the Creative Commons Attribution (CC BY) license (<https://creativecommons.org/licenses/by/4.0/>).

1. Introduction

Electrical activity recording of neural cell networks can provide wealthy information concerning the physiology, as well as physiological degeneration that may cause diseases, such as Parkinson's or Alzheimer's [1,2]. Microelectrode arrays (MEAs) have been adopted to monitor neural signals for a long time at regular intervals through electrocorticography (ECoG) [3]. The amplitude signals are larger and the higher-frequency patterns have greater resolution at the intracerebral local field potential and ECoG sites compared to scalp electroencephalogram (EEG) sites [4]. This method provides an advanced understanding of the functioning of brain activity. Moreover, ECoG can measure underlying changes in the surface of the cortex. Flexibility and biocompatibility are the primary concern related to the practical implementation of MEAs for recording in vivo data from the subject on a long term basis [5]. These conditions also allow the MEAs to be placed directly on the skull to interface with the neural system. Commonly, polyimide is applied as the base material, offering excellent biocompatibility and high flexibility for the manufacturing

of MEAs [6,7]. In the past few years, the flexible MEAs were consistently developed to stimulate and record signals from multiple neurons [8–11]. Several highly sensitive MEAs were developed using micro-electromechanical systems [12–14], a complementary metal-oxide-semiconductor [15], and lab-on-chip micro-fabrication techniques [16,17] to fabricate large numbers of electrode arrays over a small area. Moreover, to enable simultaneous and multisite recording from a large number of individual neurons, each electrode is preferred to be operated at high spatiotemporal resolution [18]. Furthermore, a precise wafer-scale process is used to fabricate MEAs with excellent uniformity, enhanced quality, and tolerance to achieve high reliability. The current research is focused on the fabrication of MEAs with advanced micro-fabrication techniques to lower down the production cost and achieve a high yield. The large wafer-scale micro-fabrication can greatly reduce the manufacturing cost due to the possibility of mass production [19].

In this work, a 6-inch-high resistivity silicon wafer was used as a supporting substrate and combined with flexible polyimide to manufacture 25 MEAs on a single wafer through mass production. Several fundamental techniques, such as surface treatment, evaporation process, and curing conditions, are adopted during the micro-fabrication process. The MEAs are designed to offer high spatiotemporal resolution throughout 60 recording channels, aiming to fulfill the requirement of neural sensors to record brain signals with high sensitivity and selectivity. The surface roughness of silicon supporting substrate, polyimide, and electrode have been analyzed by atomic force microscopy (AFM). Meanwhile, the impedance of the electrodes are measured by electrochemical impedance spectroscopy (EIS). Moreover, the fabricated MEAs are surface-mounted on well-packaged printed circuit boards (PCBs) via a slot-type connector to facilitate the signal recording process. These connectors and PCBs can be disassembled apart, whenever the signal recording session is not required. The circuitry advancement relieves patients from carrying the extra weight of connector and PCBs. Additionally, it also provides the possibility to leave the flexible MEAs on the patient skull until the next recording during in vivo test. The reliability of assembled MEAs has been characterized via EIS. In this article, a detailed step-by-step micro-fabrication process, assembly method, and measurement process has been discussed. This discussion could be beneficial for the researchers to understand wafer-scale MEAs fabrication issues.

2. Experimental Details

The wafer-scale micro-fabrication was used to process and fabricate the proposed flexible and multichannel MEAs. The fabrication process was isolated into 7 steps, as shown in Figure 1. Step 1: The silicon substrate was dipped into a 10% hydrogen fluoride solution to remove existing oxide. Afterward, the substrate is prepared for plasma treatment to enhance surface roughness using O_2/H_2 with a radio frequency (RF) power of 650 W, chuck temperature of 80 °C, chamber pressure of 2 Torr, and process time of 30 s. Substrate roughness was measured via AFM, and the root mean square (RMS) value of 8.64 nm was detected, as shown in Figure 2a. This accurate surface roughness helped to enhance the adhesion between the silicon supporting substrate and Al metal sacrificial layer [20]. Step 2: The Al sacrificial layer, with a thickness of 3 μm , was deposited by an e-beam process. Step 3: The most commonly used non-photosensitive biocompatible material (HD Microsystems, PIX1400) (HD Microsystems, Hitachi, Japan) was spin-coated on the deposited Al layer. The polyimide layer was deposited three times at 3 μm each time via a manual spin-coater with 500/3000/500 revolutions per minute (RPM) and coating time adjusted to 10/40/5 s, respectively. Subsequently, soft baking was done under 100 °C for 3 min, followed by a curing process under 300 °C for 3 min in a conventional oven. The polyimide thickness was adjusted to 9 μm to minimize the tensile stress and rectify the adhesion problem between the fabricated film and mouse skull. Afterward, a metallization process was performed to reduce rolling issues and enhance film planarization. Step 4: Photolithography was performed to create a specific pattern on the deposited polyimide layer. This process was followed by a curing process, in which the prepared structure was

placed at the ambient condition of 90 °C for 30 min and 125 °C for 60 min separately to achieve the desired shape with appropriate aspect ratio. Moreover, the polyimide surface was treated with an inductively coupled plasma etching process under a chamber pressure of 450 mTorr, a coil power of 650 W, a CF₄ flow of 8 sccm, and an O₂ flow of 72 sccm.

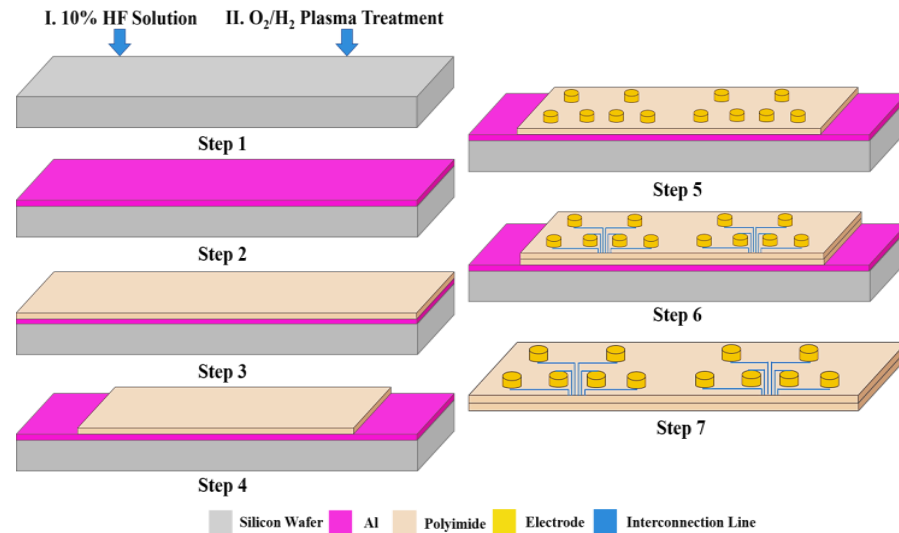
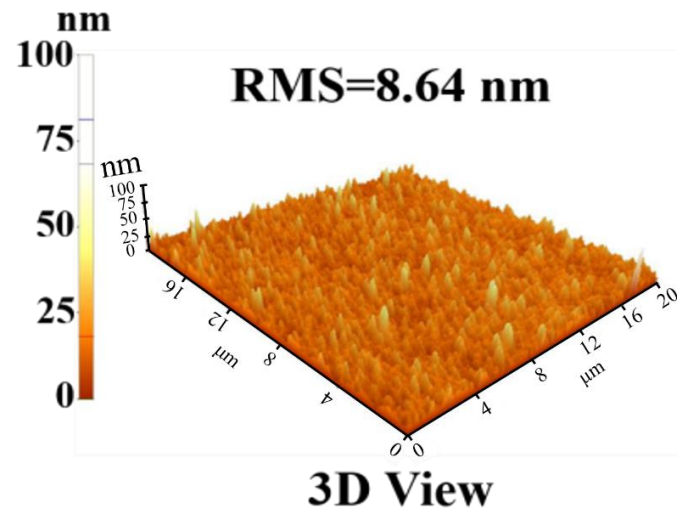


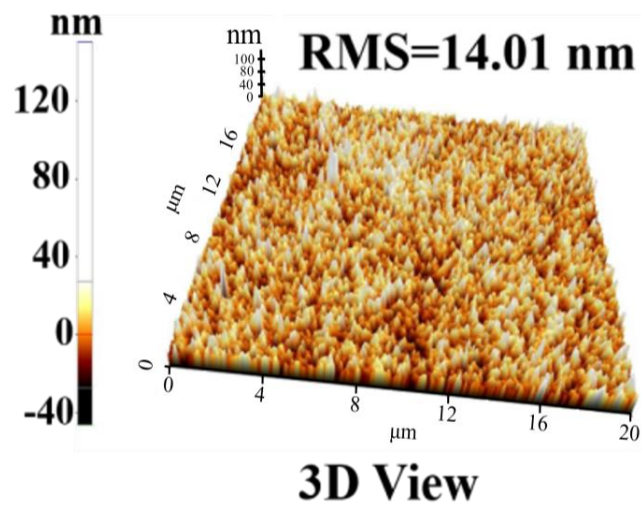
Figure 1. The fabrication schematic of the proposed flexible polyimide-based multichannel micro-electrode arrays (MEAs).

The adhesion between the first polyimide layer and Cr/Pt metal layer was due to the high RMS value of 14.01 nm, as demonstrated in Figure 2b. Step 5: 60 channels recording electrode network were formed by photolithography, in which the Cr/Pt (15/150 nm) metal layer was evaporated with deposition rates of 3/3 Å/s. Before the evaporating process, the metal source was cleaned in an ultra-sonic methanol bath and implementing isopropyl alcohol (IPA), which made the surface of electrode metal layer much smoother. Typically, source cleaning and pre-melting processes could offer a more constant composition and surface topography [20]. Subsequently, a lift-off process was executed with a pressure of 3 MPa to clean the fabricated devices first with acetone for 60 s, followed by an IPA treatment for 30 s, and, finally, deionized water (DI-water) treatment for 60 s. The roughness of the electrode surface with a low RMS value of 3.46 nm is demonstrated in Figure 2c. Step 6: The wafer was sequentially fabricated with the second polyimide film through the patterning process, similar to Step 3. The wafer was masked using photoresist to define interconnection lines and pads of the structure. After that, a 15/150 nm-thick Cr/Pt metal layer was formed by using an e-beam evaporator with a deposition rate of 3/3 Å/s. At last, the masking areas of interconnection lines and pads were stripped by a lift-off process using acetone/IPA/DI, respectively. Step 7: Wet etching was executed with an etchant of (H₃PO₄ + HNO₃ + CH₃COOH) solution to fully remove the Al layer, and, finally, the desired MEAs could be obtained.

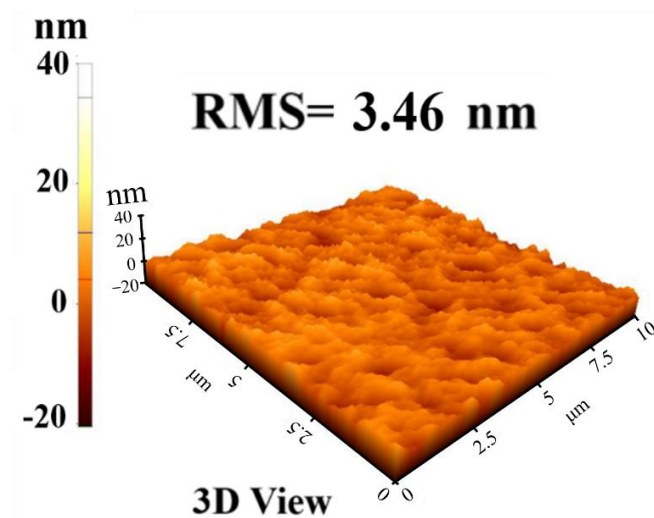
The proposed and fabricated structure of a single MEA was a fully processed 6-inch silicon wafer, as shown in Figure 3. The designed MEA was realized with a combination of three parts, named recording sites, interconnection lines, and interconnection pads. Recording sites were well arranged with high spatiotemporal resolution in a compact area. The MEAs structures were efficiently optimized to reduce the interference between the adjacent electrodes. Moreover, the advanced micro-fabrication technology helped to fabricate interconnection pads without any shorting points and enabled to transfer a reliable signal from the recording electrode sites to the detection equipment.



(a)



(b)



(c)

Figure 2. Surface roughness analyzed by atomic force microscopy (AFM): (a) Surface morphology of the silicon supporting wafer after O₂/H₂ plasma treatment; (b) surface morphology of the polyimide wafer after CF₄/O₂ plasma treatment; and (c) surface morphology of the Cr/Pt electrode layer.

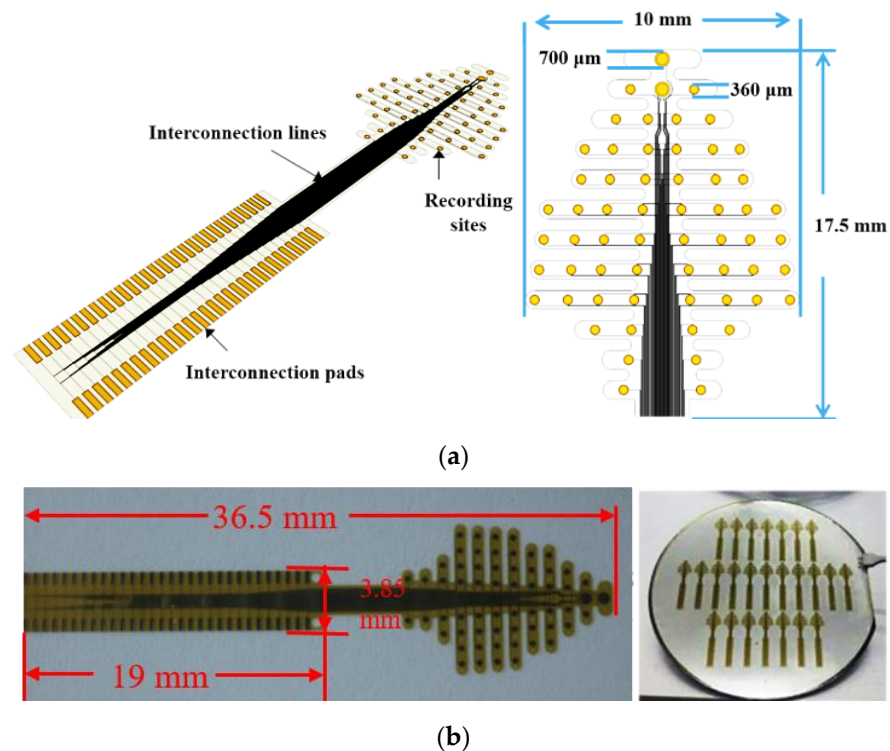


Figure 3. Images of the designed and fabricated MEAs: (a) The designed structure of a single MEA and (b) a single fabricated MEA with the fully processed 6-inch silicon supporting wafer and MEA.

The existing interconnection pads on a fabricated device were mainly added to connect with a slot-type connector. The advanced micro-fabrication method was used to fabricate 25 flexible MEAs on a single 6-inch silicon wafer. Additionally, the maximum area of exploitation was carefully considered to avoid wafer edge deflection and fabrication tolerance.

The schematic plot (a), side view (b), and top view (c) of a fully assembled flexible MEA are shown in Figure 4. In total, 60 pins were led out from the slot type connector on the top floor and connected to the interconnection pads of the bottom flexible-PCB (FPCB) through vias, 30 of which were visible, while the other 30 vias were shielded by the installed slot type connector. The practical surface mounted device was fabricated with a slot-type connector without any additional bonding wires. This formation prevented the device from electrical interconnection failure, which could be caused by skull tissues during in vivo testing. The polyimide-based FPCB structure was used to support thin layer MEA electrodes and provided protection from physical damage. The top and bottom PCBs were processed with a connector socket on the front side and interconnection pads on the backside. Similarly, the FPCB was connected with top and bottom PCBs through a V-cut, which can be easily removed during in vivo testing. Usually, the skull signal is recorded for a long duration, and sometimes several rounds of recording are executed to provide accurate and reliable measurement results. Therefore, the top PCB, bottom PCB, and slot type connectors were designed to be disassembled during the in vivo recording process. This innovative circuitry helped the potential patient to relieve the acute suffering caused by the additional weight of auxiliary components. Moreover, scalp surgery was not required between successive measurements. This innovative process can help to save cost and time and reduce the complexity, along with the patient's personal relief.

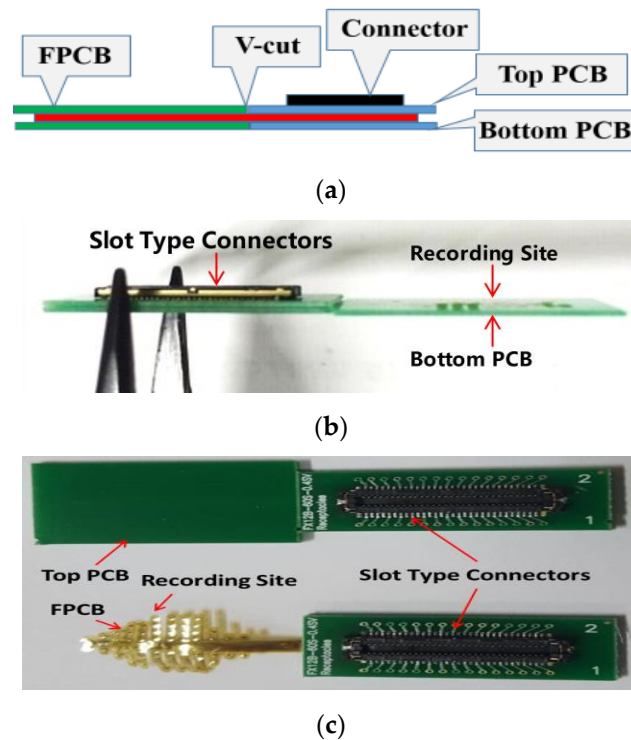


Figure 4. Images of the flexible MEAs mounted on the surface of a printed circuit board (PCB): (a) Schematic demonstration; (b) side view; and (c) top view.

3. Result and Discussion

The functionality and reliability of the proposed MEAs were investigated using the insertion of a suspended device in phosphate-buffered saline (PBS) solution, as shown in Figure 5, which improved electrical conductivity and helped to form the circuit. The electric signal of each individual channel was characterized by EIS. The measurement setup of the proposed MEAs was comprised of a signal recording system, bibulous paper, assembled MEAs as working electrodes, PBS solution, and a counter electrode.

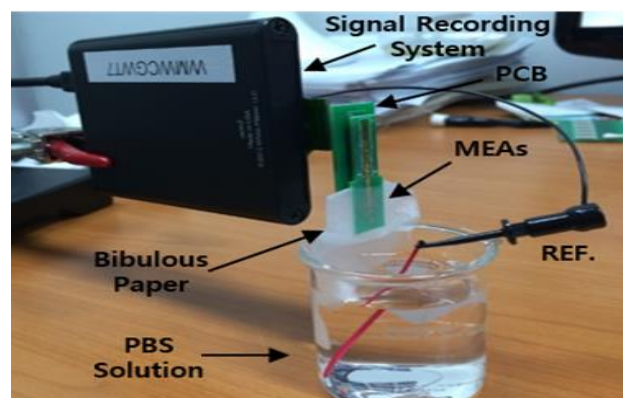


Figure 5. Measurement setup of the assembled MEAs.

Whenever metal is immersed in an electrolyte, an excess concentration of electrons forms on its surface. The interface between electrode and electrolyte remains electrically neutral, and a cloud of ions form in the electrolyte adjacent to the electrode surface [21]. When an alternating signal is applied at the input of the MEAs, the generated electrons start accelerating through the electrode surface and a charge transfer resistance is induced. The accelerated electrons overcome the ohmic resistance of bulky Cr/Pt electrodes, before reaching an electrode-electrolyte double-layer junction. The whole testing environment

can be described through Randles circuit analysis, as shown in Figure 6. The Randles circuit is comprised of a charge-transfer resistor R_{el} parallel with a double layer capacitor C_{el} , in series with an equivalent resistor of electrolyte R_{Met} and electric circuit path R_{Spread} . Due to the existence of a very large capacitance of C_{el} , R_{el} is assumed to be small in relation and can be neglected for the further study. The modified circuit is represented with a constant phase element capacitance C_{PE} and a circuit resistance R_{ms} .

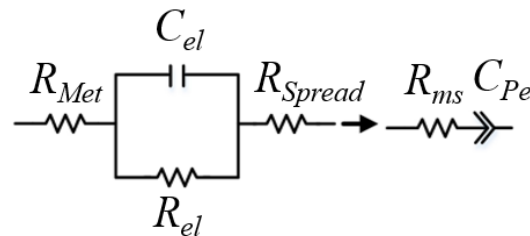


Figure 6. Schematic circuit of the electrolyte and electrode interface.

Where circuit resistance $R_{ms} = R_{Met} + R_{Spread}$

Furthermore, the representation of a simplified equivalent circuit improved the impedance of the complete electrochemical cell and can be expressed as [22]:

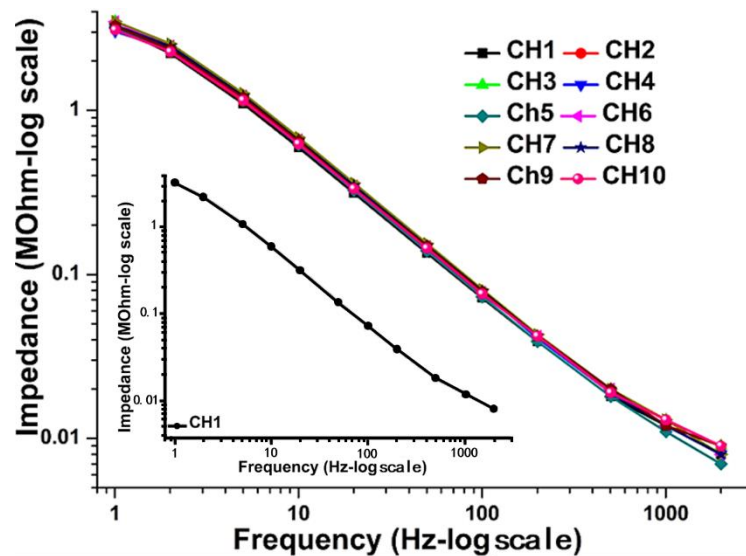
$$Z = Z_{PE} + Z_{ms} = \frac{1}{(Q2\pi f j)^n} + R_{Met} + R_{Spread} \quad (1)$$

where Q is the double layer interface capacitance in μF , f is the input frequency (Hz), and n is dimensionless. It is observed from Equation (1) that there is an inverse relationship between impedance Z and input frequency f . Hence, all impedance measurements of the proposed MEA should be followed by a given relationship. The data recording and frequency setup of the signal generator was performed using nanoZ software.

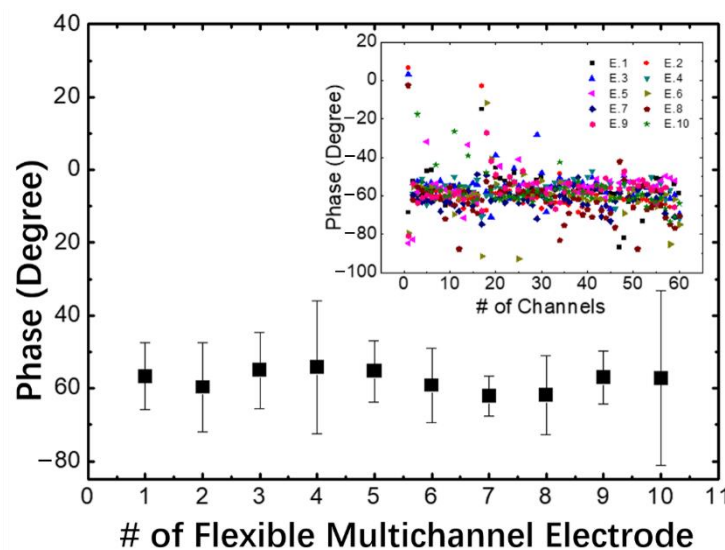
The impedance measurement of the individual channel of each MEA is important to analyze the signal to noise ratio [23]. The mean value of the measured impedance with an error bar for 10 randomly selected channels in the frequency range from 1 Hz to 2 kHz is shown in Figure 7a. The obtained results of randomly selected channels indicate the impedance magnitude of $145.6 \pm 5.4 \text{ k}\Omega$ at 100 Hz and $12.3 \pm 0.675 \text{ k}\Omega$ at 1 kHz, respectively. The phase angle was characterized at the frequency of 1 kHz, and measurements were performed for 10 MEAs. The average phase angle exhibited -57.85 ± 2.77 degrees, as represented in Figure 7b. This fruitful outcome proves a high consistency with excellent signal to noise ratio and high functionality of each individual channel in assembled MEA. Moreover, each tested channel operates efficiently with no short-circuiting or interference. However, the measured impedance results of all 10 channels were almost the same up to 1 kHz, and a slight difference emerged between 1 Hz to 2 kHz. The obtained results indicate a high correlation among 10 channels that verify the reliability and effectiveness of the advanced micro-fabrication process.

The reliability of a device is vital for the feasibility of mass-production. It also provides a guarantee for high yield and cost-effectiveness. The reliability of the fabricated MEAs was evaluated through a driven response, giving measured impedance results. The ECoG channel yield of 10 MEAs with all 60 channels is shown in Figure 8. Measurement data for 10 randomly selected MEAs with all 60 channels was recorded under a laboratory testing environment, and, afterward, the impedance results of each MEA were statistically obtained. The reduction in channel yield occurred due to fabrication failure, leakage through the polymeric encapsulation, or electric short circuit. An impedance less than 15 k Ω was considered the criteria for normally operated MEA channels versus rejected channels. The maximum ECoG channel yield of 100% was obtained at E.7, and a minimum channel yield of around 91% was observed at E.9. Based on the overall statistical data, over 90% of channels in single MEA were normally operated, which proves the excellent reliability and feasibility of the fabricated MEAs. The proposed wafer-scale fabricated

MEAs are cost-effective due to high yield percentage and can be regarded as a promising candidate to assist more researchers and doctors for further understanding of the behavior of neural networks. Additionally, it also benefits patients to treat them with a cost-effective and less painful instrument.



(a)



(b)

Figure 7. The measurement impedance and phase properties of MEAs: (a) the measured impedances of 10 random MEA channels, with the inset image of single random channels of MEAs, including the error bars; (b) the measured phase angles of the same 10 random MEAs at 1 kHz.

Furthermore, as compared with the other reported literature [24–27] and as shown in Table 1, the proposed electrode represents the low magnitude of impedance with a large area. The active area dimension of a single electrode in the fabricated MEA is $101,736 \mu\text{m}^2$, with an average output impedance of $12.3 \text{ k}\Omega$ at 1 kHz. The desired outcome represents better signal acquisition with low signal to noise ratio and provides sufficient flexibility, much smaller than the impedance required for practical implantation [22]. The acquired results of the fabricated MAE electrodes indicate magnitudes of measured impedance two orders lower, with superior signal to noise ratio. When the size of the electrodes increased,

the overall capacitance of the MEA also increased and impedance decreased. Through comparing these obtained results, it can be concluded that there should be a trade-off between the signal to noise ratio and the size of the electrode when facing a practical application [26].

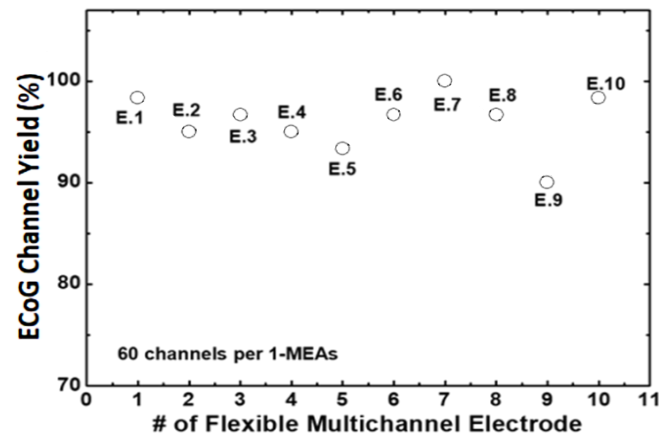


Figure 8. The electrocorticography (ECoG) channel yield measured from 60 channels per 1-MEAs.

Table 1. Performance comparison of the proposed microelectrode arrays (MEAs) with several reported MEAs.

Ref.	Electrode	Numbers of Electrodes	Electrode Size (μm^2)	Impedance at 1 kHz
[24]	Gold	8	53,066	150 k Ω
[25]	Gold	10	14,000	1 M Ω
[26]	Gold & Ti	8 & 16	125,600	18 k Ω
[27]	ITO & Pt	49	240,000	15 k Ω
This work	Cr/Pt	60	101,736	12.3 k Ω

An *in vivo* test on the skull of a hybrid adult male mouse (C57BL/6J—129S4/SvJae hybrid mice (12–15 weeks old)) was conducted to measure brain signals. The mouse was anesthetized with a ketamine (120 mg/kg, *i.p.*) and xylazine (6 mg/kg, *i.p.*) cocktail. The effect of anesthesia was monitored during the entire testing. Under the anesthetic condition, the mouse was placed on the stereotaxic apparatus (David Kopf Instruments, Model 902, Tujunga, CA, USA). The ear bars were placed in the mouse's ear canal and tightened carefully. The eyes were covered with biocompatible jelly (e.g., petroleum jelly) to protect them from drying under surgery light. Afterward, the mouse's head was moisturized with 70% ethanol and the fur was shaved from the head. Subsequently, 2% lidocaine hydrochloride was injected for local anesthesia. The head was incised about 2.5 cm inside the scalp and the skin was pinched with micro-clamps (Fine Science Tools, Inc., 18052-03, Foster City, CA, USA) to keep the incision wide open. Later, the remaining tissues and membranes were removed from the skull by using sterilized cotton swabs. After that, the bregma point was marked and MEA electrodes were placed on the skull. The electrode array was swabbed clean with alcohol and kept completely dry in order to obtain a better adhesion with a mouse skull. The electrodes remained fixed on the skull, due to Van der Waals forces. A rigid stick was positioned on the middle of the head as a strut to connect the vertical connector with a strong glue, then the dental acrylic cement was applied over the skull and the backside of the connector plane. Subsequently, the micro-clamps were removed and the incised skin was sutured. After recovery, the electrodes could be connected to the headbox of a multichannel EEG amplifier system (Synamps², Charlotte, NC, USA) via the connector and the recording was performed after 1 hour of habituation. The image of MEA electrodes placed on the mouse skull during *in vivo* test is

presented in Figure 9a,c, respectively. The electrode array had a Christmas tree structure with 12 branches on each side, and each branch had several electrical contact points, covering the exposed skull in an evenly distributed manner (Figure 9b). It is observed that the MEAs were well-arranged and conformed to the skull. This precise implantation helped to record signals after the mouse was habituated. CH1-CH10 represents the output of 10 randomly selected channel electrodes out of 60 channels. The VB and nRT as shown in Figure 9b represent the data from two big electrodes used for grounding purposes.

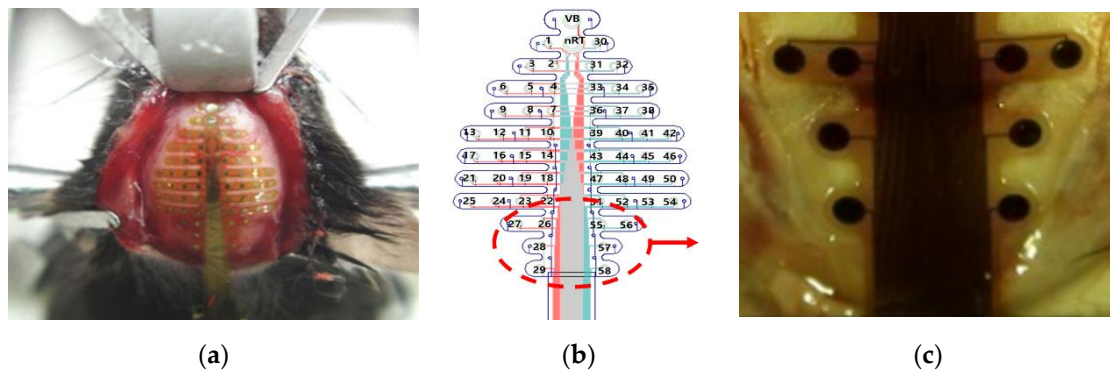


Figure 9. Images of the microelectrode: (a) Flexible MEAs mounted on the skull of an adult male mouse; (b) arrangement of the high-density mouse ECoG electrodes; and (c) microscopic photograph of the partially enlarged MEAs.

An absence seizure was recorded from the mouse skull with placed MEA by systemic administration of 50 mg/kg γ -butyrolactone (GBL) to induce bilaterally synchronous spike-wave density (SWD). The sample traces of ECoG with SWD episodes are exhibited in Figure 10, and the SWDs robustly occurred in the GBL model. The absence seizure was observed in all channels, and it was noticeable that strong signals were detected favorably in the parietal and frontal cortex.

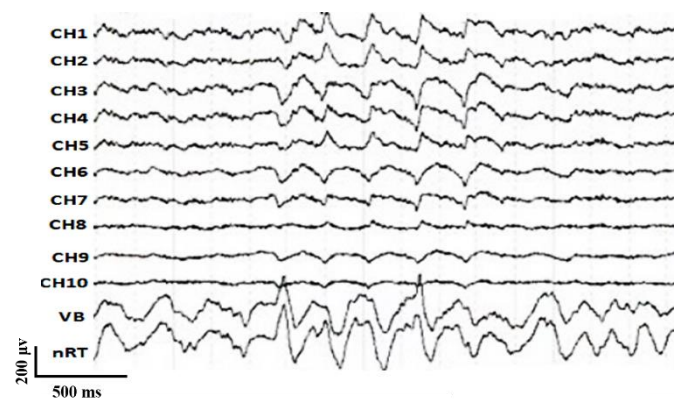


Figure 10. A sample trace of ECoG experiencing absence seizure induced by intraperitoneal injection of γ -butyrolactone (GBL). The number follows the channel montage defined in Figure 9b.

4. Conclusions

In this article, the wafer-scale fabrication and assembly method of flexible polyimide-based MEA with 60 channels is proposed. The critical fabrication technique is explicitly introduced to demonstrate the process flow with clear understanding. A group of 25 MEAs were fabricated on a single 6-inch high-resistivity silicon wafer by carefully considering the maximum area exploitation to avoid wafer edge deflection and fabrication tolerance. FPCB and a slot-type connector were applied to provide surface-mounted assembly without additional wire-bonding, representing an easier signal recording method for the fabricated MEAs. The EIS measurement was performed on 10 randomly selected channels to analyze the signal to noise ratio. The low order magnitude of impedance proves that the assembled

MEAs have excellent robustness, which could be applied to simultaneously record the neural signal with high selectivity and sensitivity. Reliability and outstanding channel yield significantly prove cost-effectiveness and give a chance for the proposed MEAs to fulfill a commercial requirement in the future biomedical market. In vivo recording on the skull of the adult male mouse demonstrates the conformation of efficient signal recording and makes this device suitable for practical application.

Author Contributions: Conceptualization, C.W., A.K., C.-P.J., and J.-H.C.; methodology, C.W., G.-F.Y., J.-H.C., and R.D.; software, A.K., Z.-L.Z., and R.D.; project administration, C.W.; validation, H.-K.S.; microfabrication, H.-K.S.; resource, H.-K.S.; formal analysis, C.W. and Z.-L.Z.; data curation, Y.-C.W.; microscope detection and analysis, Y.-C.W.; AFM measurement, C.-P.J.; EIS measurement, R.D.; in vivo test, J.-H.C.; visualization, J.-H.C.; supervision, C.-P.J., G.-F.Y., and J.-H.C.; writing—original draft, Y.-C.W.; writing—review and editing, Y.-C.W., A.K., and D.-Q.Z.; All authors have read and agreed to the published version of the manuscript.

Funding: This work is supported by the [General Financial Grant from China Postdoctoral Science Foundation] grant number [2017M611367], [Heilongjiang Postdoctoral Fund] grant number [LBH-Z17056], [National Key Research and Development Program of China] grant number [2019YFE0121800], [Natural Science Foundation of Zhejiang Province, China] grant number [2020MC2GD01], [Qianjiang Talent Plan of Zhejiang Province] grant number [2020MC2GE01], and [Major Scientific Research Project of Zhejiang Lab] grant number [2019MC0AD01, 2019MC0AB03].

Institutional Review Board Statement: All surgical and experimental procedures were performed in accordance with the institutional guidelines for the Institutional Animal Care and Use Committee, which follows Act 1992 of the Korea Lab Animal Care Regulations and associated guidelines. All efforts were made to minimize the number of animals and the animal's pain and suffering.

Data Availability Statement: The data presented in this study is contained within this article.

Conflicts of Interest: There are no conflicts of interest to declare.

References

1. Kim, R.Y.; Joo, S.H.; Jung, H.J.; Hong, N.R.; Nam, Y.K. Recent trends in microelectrode array technology for in vitro neural interface platform. *Biomed. Eng. Lett.* **2014**, *4*, 129–141. [[CrossRef](#)]
2. Wei, W.; Song, Y.; Wang, L.; Zhang, S.; Luo, J.; Xu, S.; Cai, X. An implantable microelectrode array for simultaneous L-glutamate and electrophysiological recordings in vivo. *Microsyst. Nanoeng.* **2015**, *1*, 1–6. [[CrossRef](#)]
3. Kaiju, T.; Doi, K.; Yokota, M.; Watanabe, K.; Inoue, M.; Ando, H.; Takahashi, K.; Yoshida, F.; Hirata, M.; Suzuki, T. High spatiotemporal resolution ECoG recording of somatosensory evoked potentials with flexible micro-electrode arrays. *Front. Neural Circuits* **2017**, *11*, 20. [[CrossRef](#)] [[PubMed](#)]
4. Buzsáki, G.; Anastassiou, C.A.; Koch, C. The origin of extracellular fields and currents—EEG, ECoG, LFP and spikes. *Nat. Rev. Neurosci.* **2012**, *13*, 407–420. [[CrossRef](#)] [[PubMed](#)]
5. Obien, M.E.J.; Deligkaris, K.; Bullmann, T.; Bakkum, D.J.; Frey, U. Revealing neuronal function through microelectrode array recordings. *Front. Neurosci.* **2015**, *6*, 1–30. [[CrossRef](#)] [[PubMed](#)]
6. Rousche, P.J.; Pellinen, D.S.; Pivin, D.P.; Williams, J.C.; Vetter, R.J.; Kipke, D.R. Flexible Polyimide-Based Intracortical Electrode Arrays with Bioactive Capability. *IEEE Trans. Biomed. Eng.* **2001**, *48*, 361–371. [[CrossRef](#)]
7. Constantin, C.P.; Aflori, M.; Damian, R.F.; Rusu, R.D. Biocompatibility of Polyimides: A Mini-Review. *Materials* **2019**, *12*, 3166. [[CrossRef](#)]
8. Atmaramani, R.; Chakraborty, B.; Rihani, R.T.; Usoro, J.; Hammack, A.; Abbott, J.; Nnoromele, P.; Black, B.J.; Pancrazio, J.J.; Cogan, S.F. Ruthenium oxide based microelectrode arrays for in vitro and in vivo neural recording and stimulation. *Acta Biomater.* **2020**, *101*, 565–574. [[CrossRef](#)]
9. Jackel, D.; Bakkum, D.J.; Russell, T.L.; Müller, J.; Radivojevic, M.; Frey, U.; Franke, F.; Hierlemann, A. Combination of High-density Microelectrode Array and Patch Clamp Recordings to Enable Studies of Multisynaptic Integration. *Sci. Rep.* **2017**, *7*, 978. [[CrossRef](#)]
10. Driscoll, N.; Maleski, K.; Richardson, A.G.; Murphy, B.; Anasori, B.; Lucas, T.H.; Gogotsi, Y.; Vitale, F. Fabrication of Ti₃C₂ MXene microelectrode arrays for in vivo neural recording. *J. Vis. Exp.* **2020**, *156*, e60741. [[CrossRef](#)]
11. Xie, K.; Zhang, S.; Dong, S.; Li, S.; Yu, C.; Xu, K.; Chen, W.; Guo, W.; Luo, J.; Wu, Z. Portable wireless electrocorticography system with a flexible microelectrodes array for epilepsy treatment. *Sci. Rep.* **2017**, *7*, 7808. [[CrossRef](#)]
12. Sung, H.K.; Lee, H.K.; Wang, C.; Kim, N.Y. Design and Fabrication of Implantable Neural Probes with Monolithically Integrated Light-Emitting Diodes for Optogenetic Applications. *J. Nanosci. Nanotech.* **2017**, *17*, 2582–2584. [[CrossRef](#)] [[PubMed](#)]

13. Seymour, J.P.; Wu, F.; Wise, K.D.; Yoon, E. State-of-the-art MEMS and microsystem tools for brain research. *Microsys. Nanoeng.* **2016**, *3*, 1–16. [[CrossRef](#)] [[PubMed](#)]
14. Jiang, X.; Sui, X.H.; Liu, Y.L.; Yan, Y.; Zhou, C.Q.; Li, L.M.; Ren, Q.S.; Chai, X.Y. In vitro and in vivo evaluation of a photosensitive polyimide thin-film microelectrode array suitable for epiretinal stimulation. *J. Neuroeng. Rehabil.* **2013**, *10*, 48. [[CrossRef](#)] [[PubMed](#)]
15. Ballini, M.; Muller, J.; Livi, P.; Chen, Y.H.; Frey, U.; Stettler, A.; Shadmani, A.; Viswam, V.; Jones, I.L.; Jackel, D.; et al. A 1024-Channel CMOS Microelectrode Array with 26,400 Electrodes for Recording and Stimulation of Electrogenic Cells In Vitro. *IEEE J. Solid State Circuits* **2014**, *49*, 2705–2719. [[PubMed](#)]
16. Delivopoulos, E.; Chew, D.J.; Mineev, I.R.; Fawcett, J.W.; Lacour, S.P. Concurrent recordings of bladder afferents from multiple nerves using a microfabricated PDMS microchannel electrode array. *Lab Chip* **2012**, *12*, 2540–2551. [[CrossRef](#)]
17. Tolstosheeva, E.; Gonzalez, V.G.; Biefeld, V.; Kempen, L.; Mandon, S.; Kreiter, A.K.; Lang, W. A Multi-Channel, Flex-Rigid ECoG Microelectrode Array for Visual Cortical Interfacing. *Sensors* **2015**, *15*, 832–854. [[CrossRef](#)]
18. Dragas, J.; Viswam, V.; Shadmani, A.; Chen, Y.H.; Bounik, R.; Stettler, A.; Radivojevic, M.; Geissler, S.; Obien, M.; Muller, J.; et al. A Multi-Functional Microelectrode Array Featuring 59760 Electrodes, 2048 Electrophysiology Channels, Stimulation, Impedance Measurement and Neurotransmitter Detection Channels. *IEEE J. Solid State Circuits* **2017**, *52*, 1576–1590.
19. Qiang, T.; Wang, C.; Kim, N.Y. A Compact High-Reliability High-Performance 900-MHz WPD Using GaAs-IPD Technology. *IEEE Micro. Wirel. Compon. Lett.* **2016**, *26*, 498–500. [[CrossRef](#)]
20. Wang, C.; Lee, W.S.; Zhang, F.; Kim, N.Y. A novel method for the fabrication of integrated passive devices on Si-GaAs substrate. *Int. J. Adv. Manuf. Technol.* **2011**, *52*, 1011–1018. [[CrossRef](#)]
21. Orazem, M.E.; Tribollet, B. *Electrochemical Impedance Spectroscopy*, 2nd ed.; Wiley: New York, NY, USA, 2008.
22. Jorcin, J.B.; Orazem, M.E.; Pebere, N.; Tribollet, B. CPE analysis by local electrochemical impedance spectroscopy. *Electrochim. Acta* **2006**, *51*, 1473–1479. [[CrossRef](#)]
23. Rihani, R.T.; Kim, H.; Black, B.J.; Atmaramani, R.; Saed, M.O.; Pancrazio, J.J.; Ware, T.H. Liquid crystal elastomer-based microelectrode array for in vitro neuronal recordings. *Micromachines* **2018**, *9*, 416. [[CrossRef](#)] [[PubMed](#)]
24. Kim, J.M.; Im, C.; Lee, W.R. Plateau-Shaped Flexible Polymer Microelectrode Array for Neural Recording. *Polymers* **2017**, *9*, 690. [[CrossRef](#)] [[PubMed](#)]
25. Mineev, I.R.; Lacour, S.P. Impedance spectroscopy on stretchable microelectrode arrays. *Appl. Phys. Lett.* **2010**, *97*, 043707.
26. Myllymaa, S.; Myllymaa, K.; Korhonen, H.; Djupsund, K.; Tanila, H.; Lappalainen, R. Development of Flexible Thin Film Microelectrode Arrays for Neural Recordings. In Proceedings of the 14th Nordic-Baltic Conference on Biomedical Engineering and Medical Physics, Riga, Latvia, 16–20 June 2008; Springer: Berlin/Heidelberg, Germany, 2008; Volume 20, pp. 286–289.
27. Ledochowitsch, P.; Yazdan-Shahmorad, A.; Bouchard, K.E.; Diaz-Botia, C.; Hanson, T.L.; He, J.W.; Seybold, B.W.; Olivero, E.; Phillips, E.A.K.; Blanche, T.J.; et al. Strategies for optical control and simultaneous electrical readout of extended cortical circuits. *J. Neurosci. Methods* **2015**, *256*, 220–231. [[CrossRef](#)] [[PubMed](#)]